Modeling of charge-mass transport in solid electrolyte-based electrochemical nanomanufacturing process

Modeling of Charge-Mass Transport in Solid Electrolyte-Based Electrochemical Nanomanufacturing Process

Keng Hsu
The Polytechnic School
Fulton Schools of Engineering
Arizona State University
7171 E. Sonoran Arroyo Mall,
Mesa, AZ 85212
Keng.h.hsu@asu.edu

Nicholas Fang
Department of Mechanical Engineering
Massachusetts Institute of Technology
77 Massachusetts Ace.,
Cambridge, MA, 02139
nicfang@mit.edu

Gautam Panikkar
The Polytechnic School
Fulton Schools of Engineering
Arizona State University
7171 E. Sonoran Arroyo Mall,
Mesa, AZ 85212
Gautam.Panikkar@asu.edu

Placid Ferreira
Department of Mechanical Science and Engineering
University of Illinois at Urbana Champaign
1206 W. Green st.,
Urbana, IL, 61801
pferreir@illinois.edu

ABSTRACT

A numerical model was developed to capture the charge-mass transport in electrochemical nanomanufacturing process based on mixed-conducting solid electrolyte material systems. This

model was verified by the matching of numerical prediction and experimental measurements of process current. The model was also used to predict parameters affecting ionic current flow, and to study the temporal and spatial transport properties of solid electrolyte silver sulfide during an electrode dissolution process. Conditions in which phase separation could occur in silver sulfide were found. Enhanced transport properties due to confinement in lateral dimensions were also observed through the developed model.

1. INTRODUCTION

1.1 Background

The unique nature of ionic transport is not only the origin of physical and chemical phenomena but the core of a wide range of applications such as manufacturing, energy conversions, and sensing techniques. The materials in which ionic transport can take place include liquid electrolyte, polymers, amorphous glasses, as well as crystalline solids. Sharing the same coupled mass-charge transport properties with their liquid counterpart, solid-state ionic materials, such as silver sulfide and copper sulfide, have seen increasing research efforts in the area of understanding their transport physics, and developing their applications in memory devices, sensing, and actuation[1-6]. One unique application is the use of solid electrolytes as a tool for direct patterning of metals in the nano-scale [7-10]. First introduced by the authors, this method creates sub-50 nanometer resolution features using the solid contact-based anodic dissolution of a metal substrate in contact with the pre-patterned solid electrolyte stamp as depicted in Figure 1.

To fully exploit this process for development of a nanomanufacturing process, a complete understanding of the transport physics of the species involved is necessary in order to

gain control of substrate quality, yield, and explore process capability. Silver sulfide is known to be a mixed-electronic-ionic conductor with an electronic conduction bad gap of ~1.3eV. The decoupling of such mixed conduction into its electronic and ionic component has historically been carried out by setting up the respective Nernst-Planck equations of the electronic and ionic species. These equations are setup under the relations between chemical potentials and electrochemical potentials only pertain to the silver sulfide compound. Under special end conditions such as fully-blocking and fully-reversible conditions for either electronic or ionic species, these equations can be solved analytically. In fully-blocking boundary conditions, either the ionic or electronic specie is blocked from passing through an interface. However, none of these conditions are seen in practical applications that involves electrode reactions [11-12].

In this letter we introduce a numerical model to gain insight into the transient behavior of the ionic transport in solid electrolyte silver sulfide, Ag_2S, under these conditions: ionic transport in the electrolyte domain dominant and reaction on the metal-solid electrolyte interface dominant.

1.2 Model Set up

1.2.1 Mixed electronic-ionic conduction in Ag2S

In beta-silver sulfide, the conductivity of electrons is higher than that of silver ion in silver sulfide by about 3 orders of magnitude. This situation is realistically similar to that of an electrochemical environments where a supporting electrolyte with much higher conductivity is used. Under these conditions, the charge transport is mainly carried by the supporting electrolyte and the transport of the specie considered is mainly diffusive but with some migrative flow due to the finite conductivity of the supporting electrolyte. The transport of

silver ions from silver dissolution in silver sulfide is similar to this picture. Most of the charge transport is carried by the electrons in the system, and the transport of silver ions is mainly diffusive but with some migrative contribution due to the finite conductance of electrons. This process can be modeled by setting up a Nernst-Planck equation for the silver ions and a DC conduction for the electrons to reflect the experimental conditions where a DC constant voltage is applied and the total current is measured. The two equations are then coupled by the relation unique to silver sulfide which describes the dependence of the electronic conductivity on the chemical potential of silver in silver sulfide.

$$\frac{\partial c_{Ag}}{\partial t} = \nabla \left\{ -D_{Ag} \nabla c_{Ag} + \mu_{Ag} F c_{Ag} \nabla V \right\}$$ .....Equation 1

$$-\nabla \left(\sigma_e \nabla V - J^{ext} \right) = 0$$ .....Equation 2

and $$\sigma_e = \sigma_e^0 \left(1 + \frac{c_{Ag}}{c_{Ag}^0} \right)$$ .....Equation 3

where c_{Ag}, c^0_{Ag}, D_{Ag}, μ_{Ag} are the concentration, intrinsic concentration, diffusivity, and mobility of silver in silver sulfide respectively. σ_e is the electronic conductivity of silver sulfide, F is Faraday's constant, and V the applied voltage to the system.

A simulation domain whose geometry and dimension resembles the "solid electrolyte Pellet" shown in Figure 2 is constructed in COMSOL in which the governing transport equation (equation 1), direct-electronic current (equation 2), and dependence of the electronic conductivity of silver sulfide on silver ion concentration (equation 3) are applied. In the domain the transport of species is set to be an ionic species (silver ions) whose transport is enabled by the finite conductance of the direct electronic current in the domain. Detailed initial and

boundary conditions are described in section 2.3.

1.2.2 Silver-Silver Sulfide Interface Kinetics

When two solid surfaces are brought into contact, the actual contact between the two surfaces depends very much on the topography of the two, and is usually different from the apparent contact area. Here the actual contact area is, on the scale of the roughness of the surfaces, the points on the asperities of the two surfaces that are in actual contact, and the apparent contact area is the overall size of the surfaces of concern. The metal-solid electrolyte contact of the Ag-Ag_2S system is this nature. As seen in Figure 3, the surface activity of silver in contact with silver sulfide can consist of five processes [13]: adatom formation at a rate constant k_1, surface diffusion of surface adatoms at rate k_2, oxidation of adatoms at the actual contact points at a reaction rate constant k_3, the incorporation of reaction product silver ions across the lattice boundary into the silver sulfide lattice at a rate k_4, and the transport of these ions away from the interface at a rate k_5. The formation of adatoms from the defects of the metallic substrate provides abundance of surface adatoms that are mobile on the metal surface. When these surface adatoms reach actual contact points of the interfacial area, the oxidation reaction of these adatoms takes place and silver ions and electrons are generated from the reaction.

The rate constants associated with each of these processes can become rate limiting in different conditions. In the conditions of interest here, however, the surface diffusion rate k_2 and incorporation rate k_4 are usually orders of magnitude higher than the rest [14-17]. Therefore, the S4 etch rate is governed by k_1, k_3, and k_5, which are the adatom formation, silver oxidation, as well as ionic transport rates respectively. These rates are usually expressed as

$$k_1 \propto \exp\left(-E_A \Big/ k_B T\right)$$ .....Equation 4

$$k_3 \propto \exp\left(nFV^0 \Big/ RT\right)$$ .....Equation 5

$$k_5 \propto \sigma_{Ag} \propto n \exp\left(-(h+u) \Big/ k_B T\right)$$ .....Equation 6

where k_1 is the adatom formation rate, E_A is the activation energy for such process, k_3 is the silver oxidation rate, V^0 is the overpotential experienced by the silver atoms on the interface, k_5 is the transport rate of silver in silver sulfide. For reaction constant k_3, consider the oxidation reaction at the Ag-Ag_2S interface

$$Ag_{ada} \underset{k_{3b}}{\overset{k_{3f}}{\rightleftharpoons}} Ag_s^+ + e^-$$

The electrical current density from the reaction can be expressed as

$\frac{i_a}{nFA} = \nu_f = k_{3f} \cdot c_{ada}(0,t)$ for anodic direction flow, and

$\frac{i_c}{nFA} = \nu_b = k_{3b} \cdot c_{Ag_s^+}(0,t)$ for cathodic direction flow. The new current density is then the sum of the two and can be written as

$$i_{react} = i_a - i_c = nFA\left(\nu_f - \nu_b\right) = nFA\left[k_{3f} \cdot c_{ada}(0,t) - k_{3b} \cdot c_{Ag_s^+}(0,t)\right]$$

.....Equation 7

In the case of potentiostatic conditions and considering the k_2, k_4 >> k_1, k_3, k_5 (activation energy for adatom diffusion ~0.1eV, rate of silver incorporation into silver sulfide ~10^{16} atoms/cm^2s) [14-17], the total reaction current can be simplified to

$$i_{react} = nFA\left[k_{3f} \cdot c_{ada} - k_{3b} \cdot c_{Ag^+}(0,t) \right]$$ ....Equation 8

This expression states that the reaction component of the total current measured by the potentiostat is a function of the adatom concentration on the interface region, and the temporal profile of the silver ion concentration at the Ag-Ag_2S interface. The forward and backward reaction constants in equation 1 are a function of externally applied electrical potentials and can be analyzed in the following manner.

The free energies of anodic and cathodic reactions are of the form

$$\Delta G_a^* = \Delta G_{0a}^* - \beta F\left(V - V^0\right)$$... Equation 8a

and

$$\Delta G_c^* = \Delta G_{0c}^* + (1-\beta) F\left(V - V^0\right)$$... Equation 8b

where ΔG_{0a}^* and ΔG_{0c}^* are the standard free energy at equilibrium, β is the transfer coefficient, and the term (V - V^0) denotes the anodic overpotential. The rate constants are related to the free energies and can be expressed as

$$k_{3f} = A_f \exp\left(\frac{-\Delta G_{0a}^*}{RT} \right) \exp\left[\frac{-\beta F\left(V - V^0\right)}{RT} \right]$$... Equation 8c

for the forward reaction constant and

$$k_{3b} = A_b \exp\left(\frac{-\Delta G_{0c}^*}{RT} \right) \exp\left[\frac{(1-\beta) F\left(V - V^0\right)}{RT} \right]$$... Equation 8d

for the backward reaction constant

Defining k^0 as the rate constant at equilibrium conditions, the forward and backward

reaction constants can be simplified to

$$k_{3f} = k^0 \exp\left[\frac{-\beta F\left(V - V^0\right)}{RT}\right] \text{... Equation 8e}$$

and finally

$$k_{3b} = k^0 \exp\left[\frac{(1-\beta) F\left(V - V^0\right)}{RT}\right] \text{... Equation 8f}$$

substituting these two expressions into equation 1, we obtain the expression that describes the electrical current associated with the silver dissolution reaction on the interface.

$$i_{react} = nFAk^0\left[c_{ada} \cdot e^{\frac{-\beta F\left(V-V^0\right)}{RT}} - c_{Ag^+}(0,t) \cdot e^{\frac{(1-\beta)F\left(V-V^0\right)}{RT}}\right] \text{.....Equation 9}$$

In this expression, one can observe that reaction current is linearly proportional to the changes in the adatom concentration and the silver ion concentration at the interface. It also follows exponentially with the changes in the overpotential on the anodic surface. The constant k^0 is typically in the range of 0.01 ~ 0.1m/s and β is typically 0.5. The adatom concentration c_{ada} is only a function of temperature when the composition of the metal surface is fixed. The last term, $c_{Ag^+}(0,t)$, in this equation is the concentration of silver ions at the interface. It is the term that couples the kinetics of silver dissolution reaction with the transport of silver in the silver sulfide domain.

2.3 Experimental Conditions and Computational Model Setup, Properties, and End Conditions

Figure 2 shows the experimental configuration for measuring the reaction current

during the electrode dissolution on the Ag-Ag_2S interface. The crystal is shaped to have a 1mm-mesa at the tip of the cone lathed from a 3mm diameter silver sulfide crystal synthesized by the method mentioned in our earlier work [9-11]. The crystal is held by an aluminum holder in two places as shown in the figure where the electrical contact was provided. The silver electrode was prepared by electron-beam evaporation of 400nm-thick silver onto a glass cover slip seeded with 1nm of Cr for adhesion. The electrical potential was applied by a potentiostat (Gamry R600) at the same time the electrical current recorded.

The material properties as well as the source of the data acquired are tabulated in Table 1. The intrinsic charge carrier number is used as the initial condition for concentration. Einstein's relation is used to evaluate the mobility of silver in silver sulfide.

The ionic conductivity in silver sulfide is known to have originated from its ability to deviate from its perfect stoichiometry: from $Ag_{1.998}S$ to $Ag_{2.002}S$. This implies that the charge carrier concentration of a silver sulfide stamp of perfect stoichiometry will have 0.1% of the total silver in silver sulfide becoming available for carrying ionic current. The intrinsic ion concentration here is obtained by first calculating the amount of silver (87.06% of molar mass of Ag_2S) in silver sulfide (molar mass 247.8 g/mole) followed by calculating the mole volume of this silver amount with the density of silver sulfide (7.234g/cm^3). The inverse of the molar volume gives the total amount of silver in silver sulfide; and 0.1% of this amount is then the intrinsic charge carrier concentration in silver sulfide.

2. DISCUSSION

By using the intrinsic silver concentration [13] in the solid electrolyte domain and a silver ion influx obtained experimentally to solve $c_{Ag^+}(0,t)$ for the temporal distribution of the

concentration of silver ions at x=0 (1-D) or on the interface, we were able to examine the effects of physical properties of the system on the electrical current during a dissolution process. Figure 4 shows the electrical current measurements of electrode dissolution processes carried out with solid electrolyte pellets of different intrinsic states, and the calculation results based on the developed model. The property difference between the two cases is that the silver side of a crystal has higher silver concentration and is usually close to the upper bound of the stoichiometry of silver sulfide $Ag_{2.002}S$, whereas the sulfur side is the opposite. We observe that the use of a "sulfur side" stamp gives rise to larger ramping of current, shorter time constant, and higher maximum current (circles), as compared to using a "silver side" stamp (squares). The two solid lines are predicted by the developed model.

In Figure 5(a), one can see that relative differences between adatom concentration and intrinsic silver ion concentration have large effects on maximum value of the reaction current, but has little effect on how much it can increase within a given amount of time. The relative amount of these two terms determines the chemical potential available for the oxidation reaction to overcome its energy barrier, but does not have much effect on how the product silver ions from the reaction can be accommodated into the electrolyte domain. In Figure 5(b), it can be seen that the intrinsic concentration of silver ion in silver sulfide can influence the amount of ramping in reaction current. The more intrinsic Ag ions in the domain, the more concentration change can take place, resulting in more reaction current increase in a given amount of time. In Figure 5(c) and (d) it can be seen that the two quantities have an effect on ramping time constant of the reaction current, or the time constant for the S4 system to reach a steady state. The increase in overpotential can significantly increase i_{max} and shorten the time

constant in which the steady state of the system is reached, and faster diffusion (and mobility since the diffusivity and mobility of silver are relate by the Einstein relation) can also give rise to a shorter time constant: the forward reaction rate follows exponentially with anodic overpotential, and it is reflected in the reaction current increase. While the rate of transport of product silver away from the interface has much less effect on maximum current, the time constant of reach steady state can alter noticeably when the transport of silver ions is changed. This effect is demonstrated in our experimental results shown in Figure 6 where the current ramps to a higher steady value as the applied voltage increase. As the same time, the ramping time constant decrease with higher voltage as predicted earlier in the discussion.

Using the numerical model developed, we also studied the spatial and temporal properties of the ionic transport in the silver sulfide pellet. For simplicity, in these studies a constant silver influx of $4x10^{-4}$ mole/m^2s at an electrical potential of 400mV on the silver-silver sulfide interface was assumed. Figure 7 shows the numerical results three quantities studied: the instantaneous spatial distribution of the stoichiometry of silver sulfide stamp (color map), electrophoretic flux of silver species (arrows), and electrical potential distribution (contour lines). All three quantities are presented at fours temporal point of importance- 0 second, 95 seconds (during metal etching), 105 seconds (right after metal has been depleted), and 300 seconds when the process is terminated. As evident in the results, the electrode configuration induces a distortion of the electrical potential distribution and caused uneven distribution of cathodic reaction, and silver transport and accumulation is mainly toward the leading edge of the electrode on the sides. As a direct result of this, the stoichiometry at 300 seconds in a small region of the silver sulfide domain close to the leading edge exceeds the solubility limit of silver

in silver sulfide, $Ag_{2.002}S$. The implication of this is that precipitation of silver from silver sulfide can happen, giving rise to phase separation in the solid electrolyte.

It is generally recognized that the transport properties of ionic systems experiences increase when the dimensions of the domain wherein the transport takes place are small as compared to dimensions of the space charge layers or the characteristic length of the diffusive transport. Here in the developed model features of lateral dimensions ranging from 10nm up to 100nm were investigated. It is found that the with a constant potential and ion concentration imposed on the end of these nano features (which represents the interface of a solid electrolyte stamp and a metallic substrate), the potential gradient as well as the concentration gradient existed in those features increase as the lateral dimension of the features decreases as can be seen in results shown in Figure 8. From the result, it is also seen that the transport along the length of those features, also increases as the lateral dimension of the feature goes down. The migrative flux increases by nearly 60% when the width of the feature reduces from 100nm to 10nm. Similar trend is also observed in the diffusive flux. These results suggest that in terms of patterning efficiency, smaller features are preferable for the S4 process: the silver dissolution rate at the metal-solid electrolyte interface is limited by the transport properties of silver ions in the solid electrolyte domain, the faster the ions produced from the reaction can be carried away by migration and diffusion, the higher the rate of dissolution can reach under the same driving electrical potential. Our future work will focus on experimentally verify these predictions.

This work is supported by the National Science Foundation under NSF Award # 1200780 (CMMI) Direct Patterning of Metallic Nanostructures for Bio-sensing Substrate Production.

3. CONCLUSION

A numerical model has been developed to capture the transient behavior of mass-charge transport in a mixed conductor between the two steady-state conditions: interfacial kinetics dominant and ionic transport dominant. This model captures the process behavior observed experimentally in systems under different conditions. The developed model were also used to find conditions under which phase separation and damage to the patterning solid electrolyte tool can occur. The model developed here not only is useful for study of the electrode kinetics of solid-solid electrolyte systems, it can also find applications in study of electrode design in batteries.

4. FIGURE CAPTION

Fig. 1 Solid-State Superionic Stamping, S4, process and example results. (a), (b) Principle and process steps of S4 process. (c), (d) SEM micrographs of the solid electrolyte stamp and the resulting substrate. (e) Example nanostructures.

Fig. 2 Experimental solid electrolyte stamping tool configuration.

Fig. 3 Interfacial processes on a solid electrolyte-reactive metal surface

Fig. 4 Experimental mixed-electrical current evolution in a typical stamping process.

Fig. 5 Mixed-electrical current behavior predicted by the proposed model.

Fig. 6 Experimental mixed-electrical current evolution at different applied external bias.

Fig. 7 Spatial characteristics of charge and mass transport predicted by the proposed model.

Fig. 8 Solid electrolyte domain size enhancement effect on ionic transport.

5. FIGURES

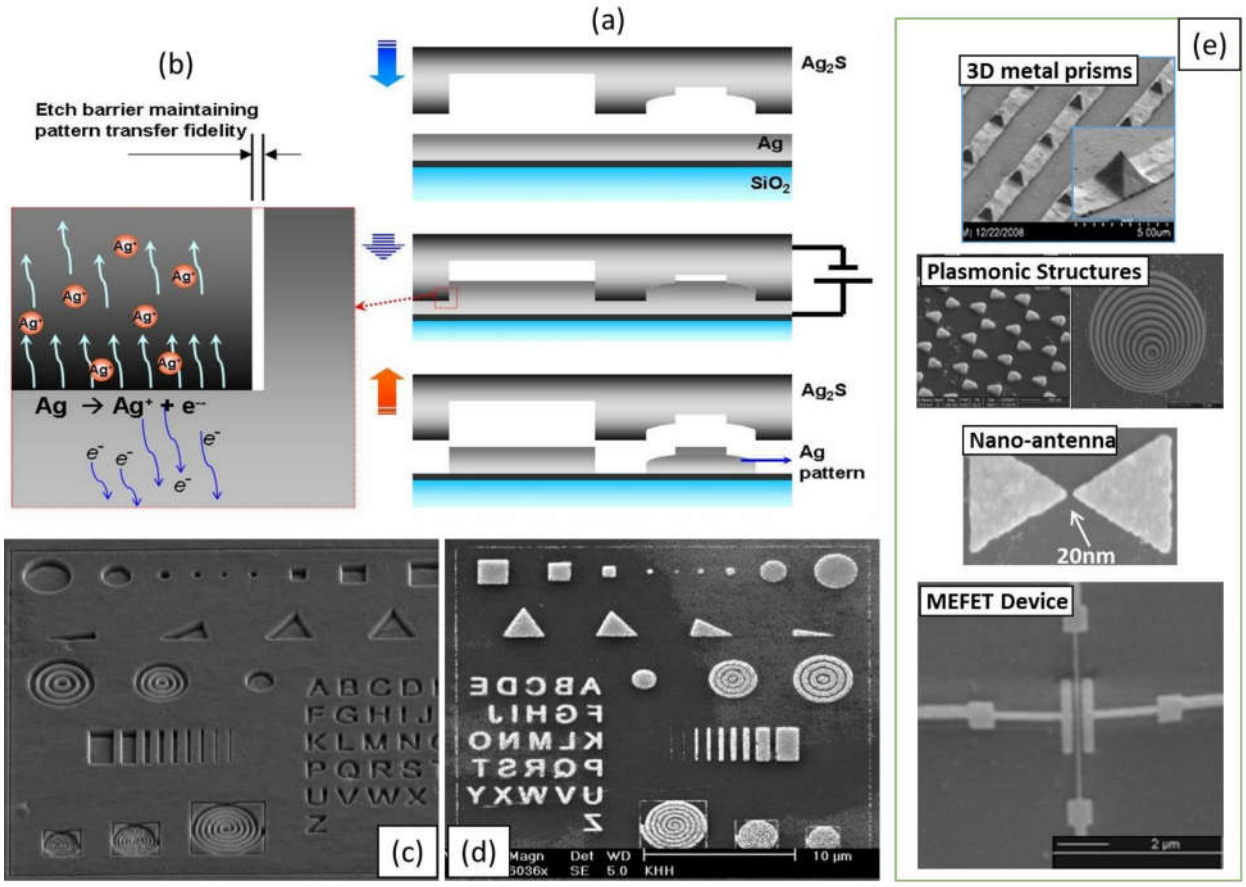

Fig. 1 Solid-State Superionic Stamping, S4, process and example results. (a), (b) Principle and process steps of S4 process. (c), (d) SEM micrographs of the solid electrolyte stamp and the resulting substrate. (e) Example nanostructures.

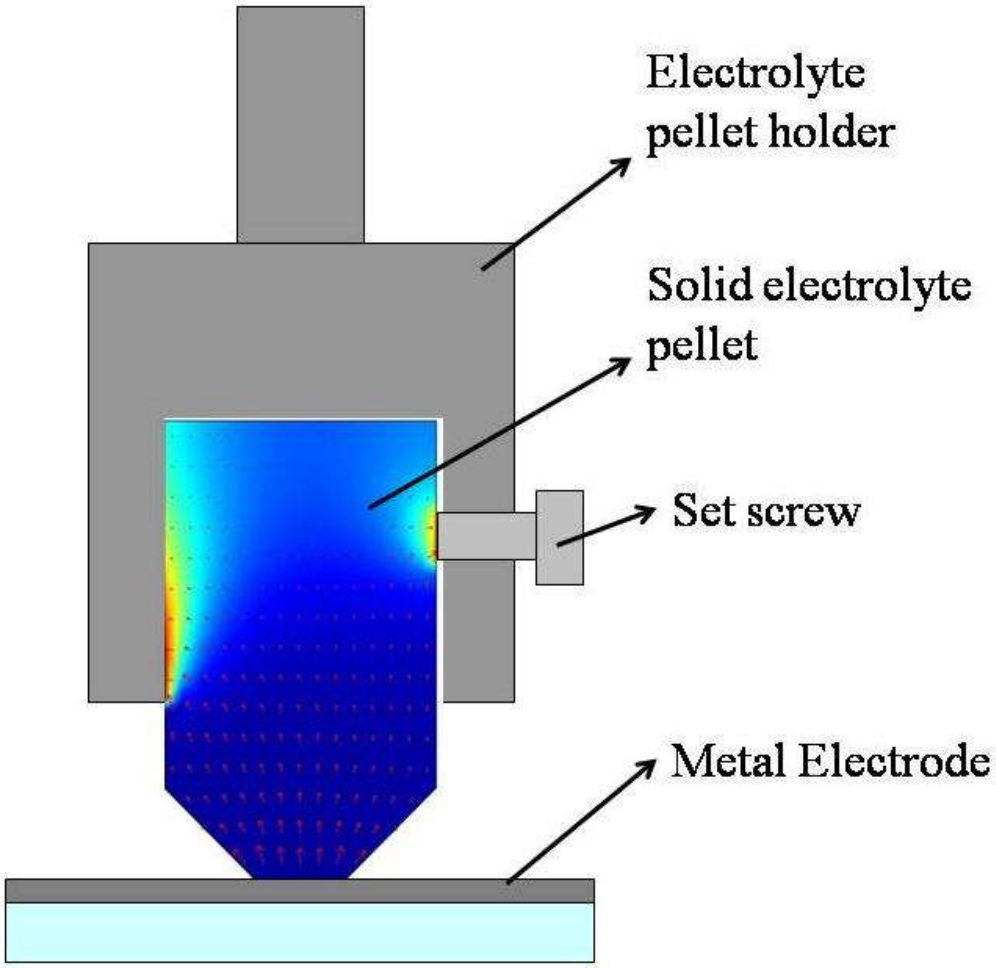

Fig. 2 Experimental solid electrolyte stamping tool configuration.

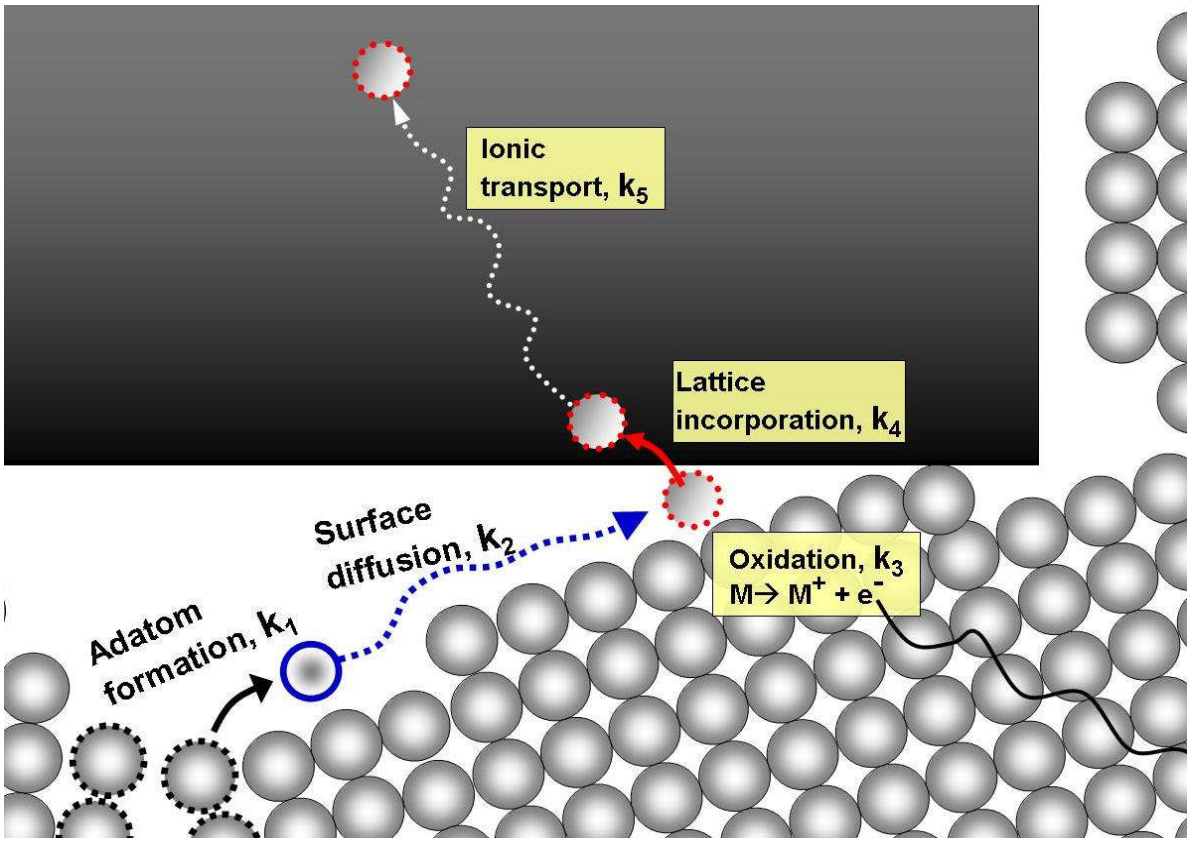

Fig. 3 Interracial processes on a solid electrolyte-reactive metal surface

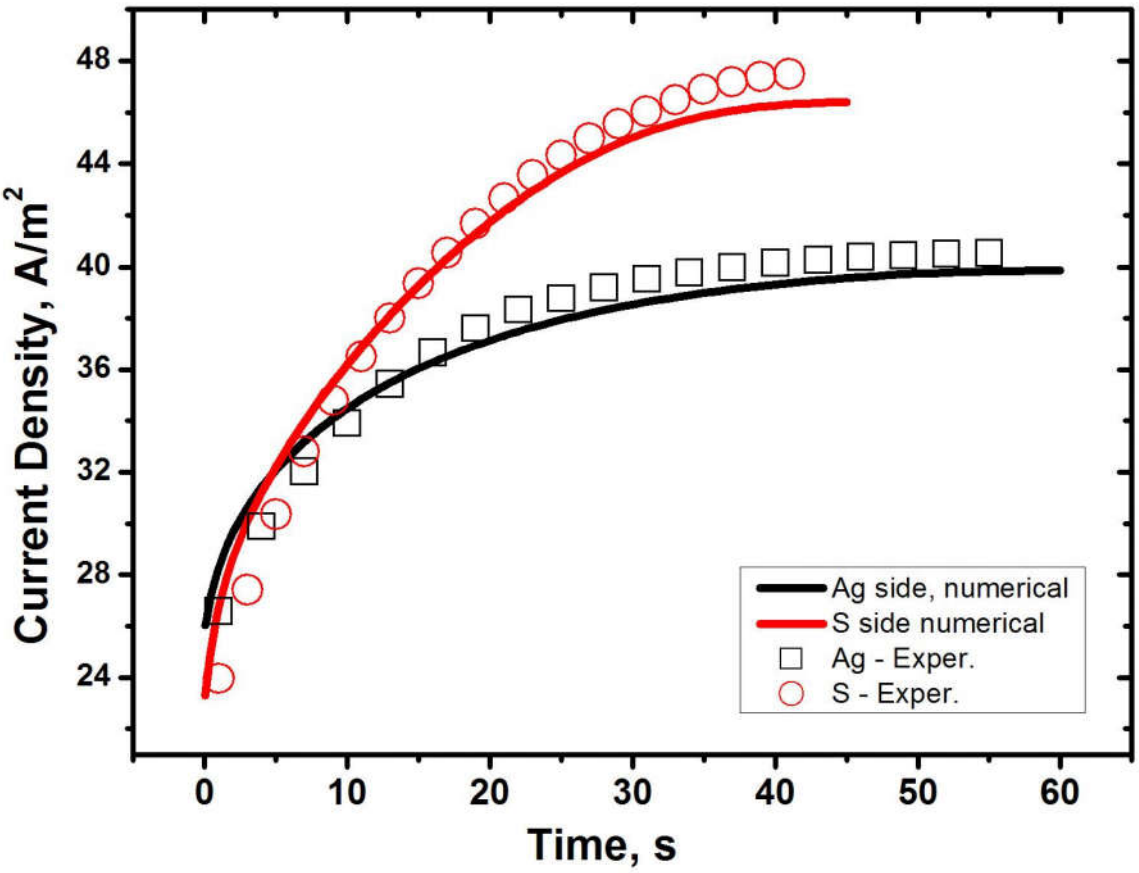

Fig. 4 S4 Process current evolution.

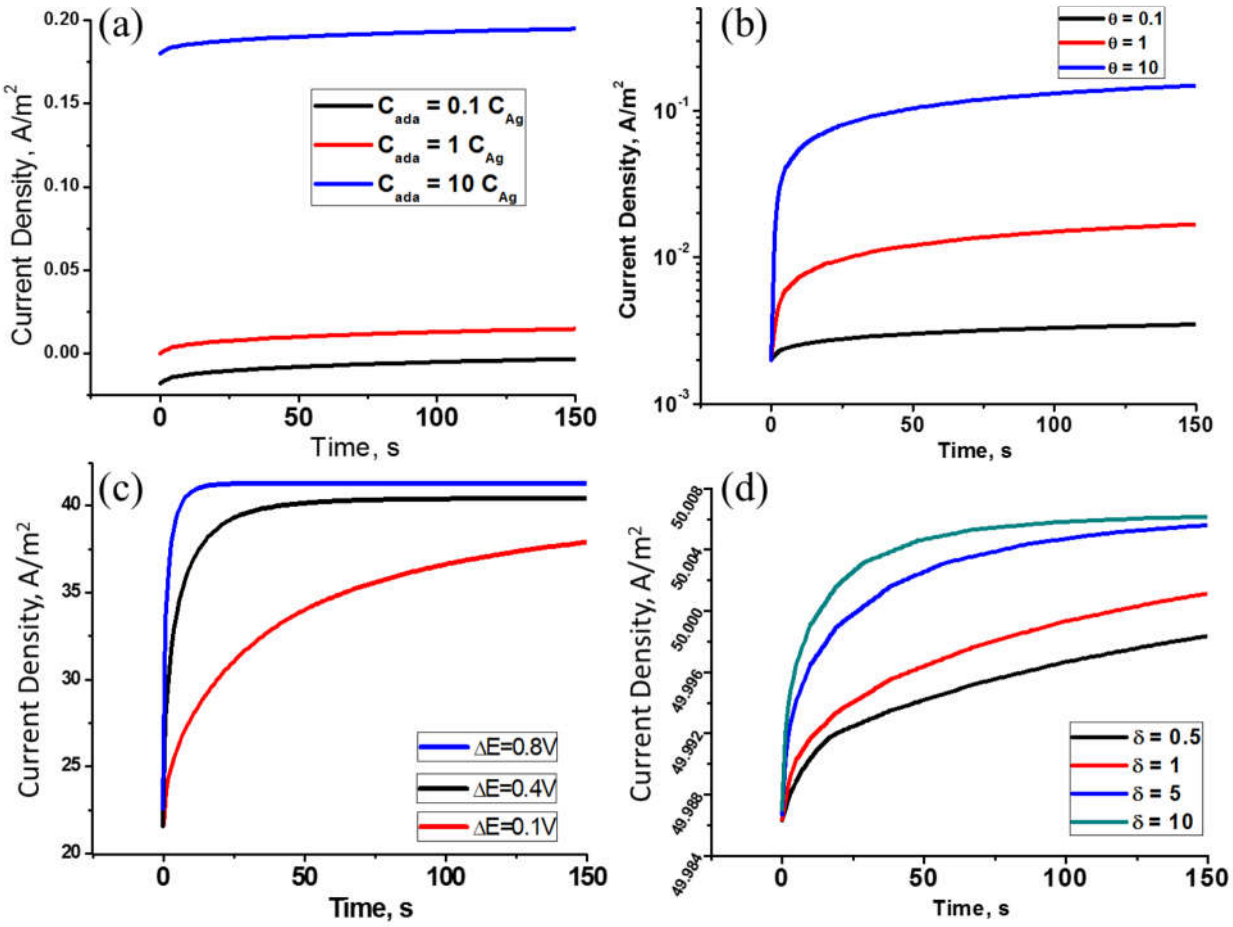

Fig. 5 Process current behavior predicted by the developed model.

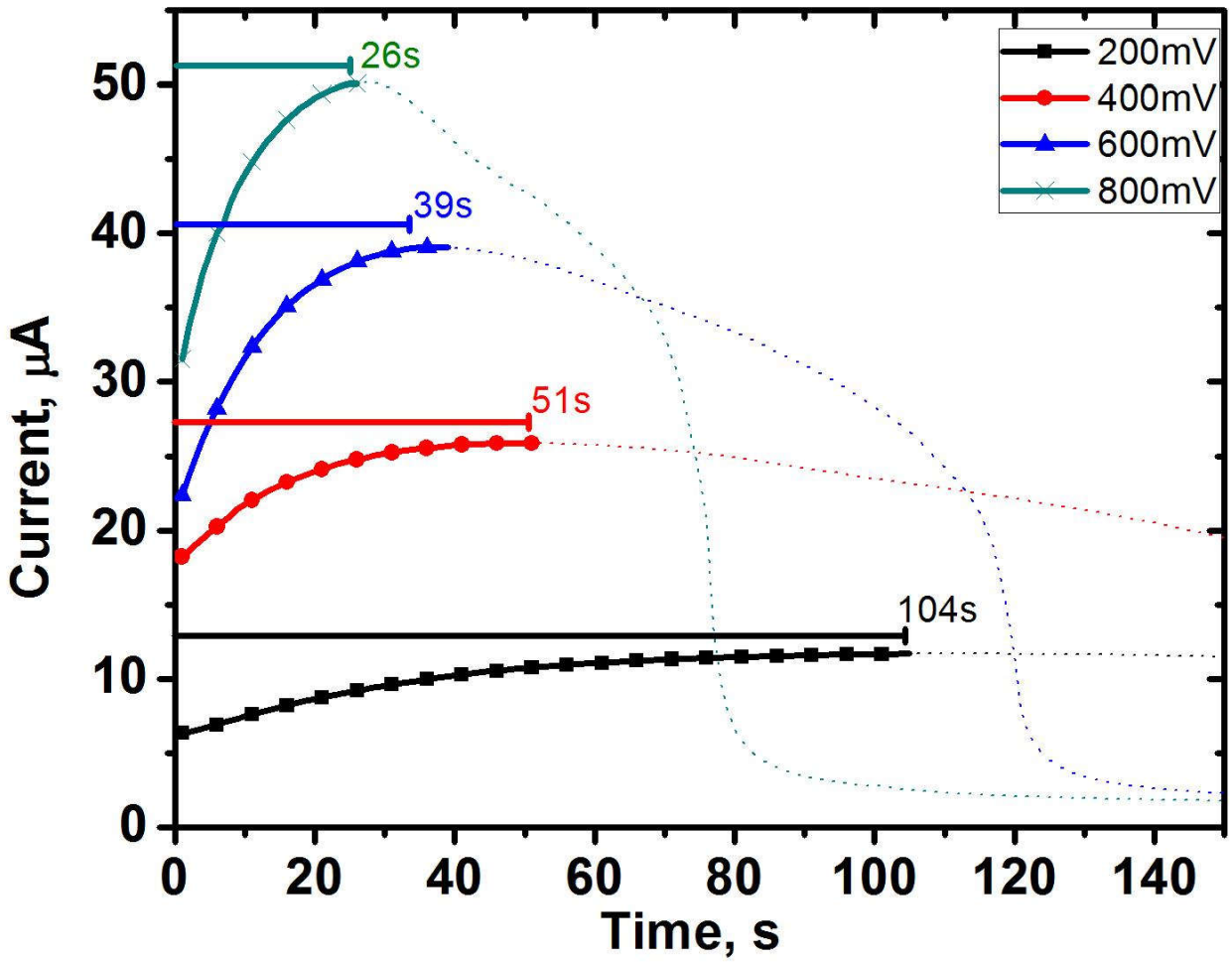

Fig. 6 Experimental process current evolution at different applied external bias.

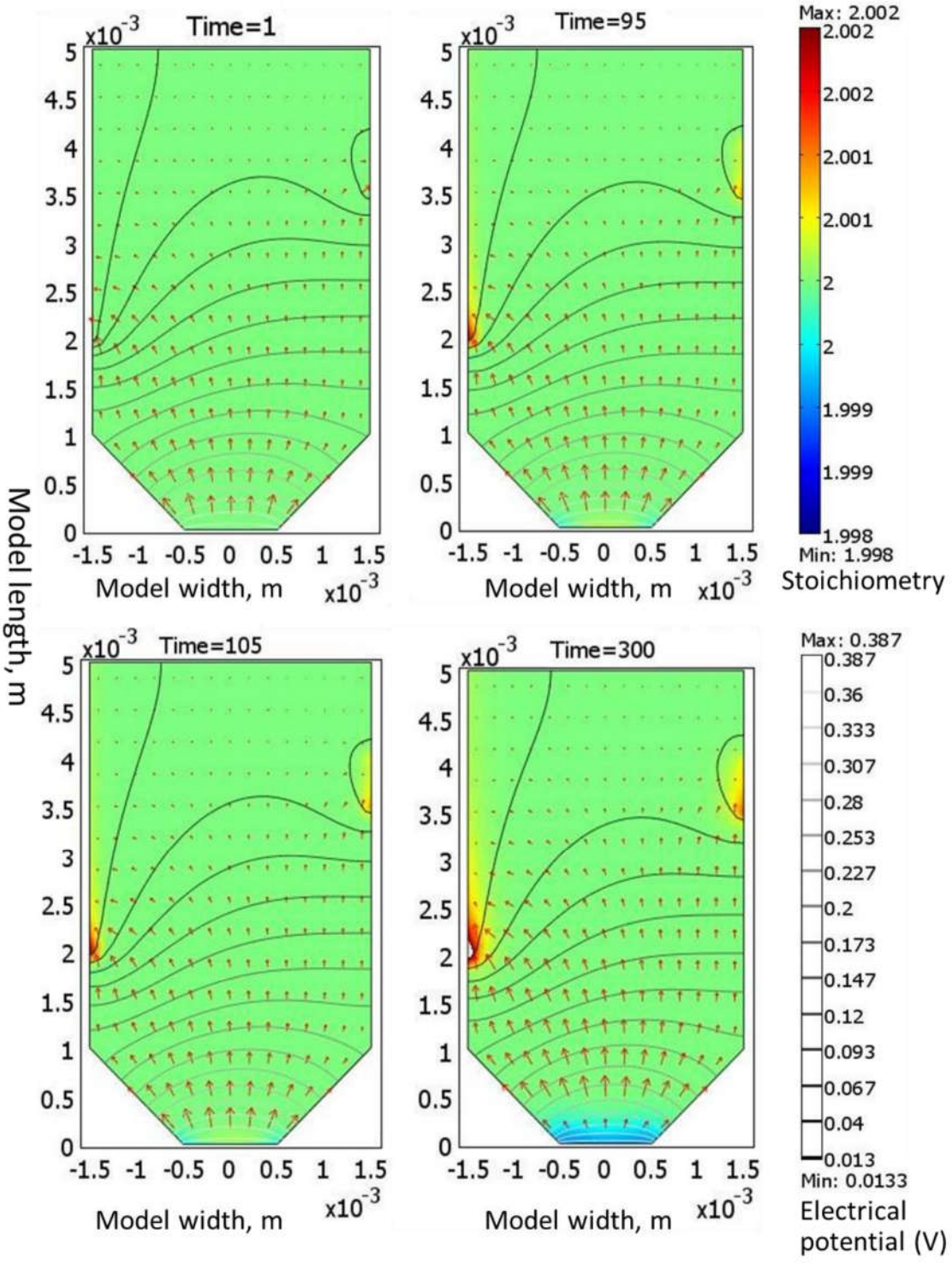

Fig. 7 Spatial characteristics of charge and mass transport predicted by the developed model.

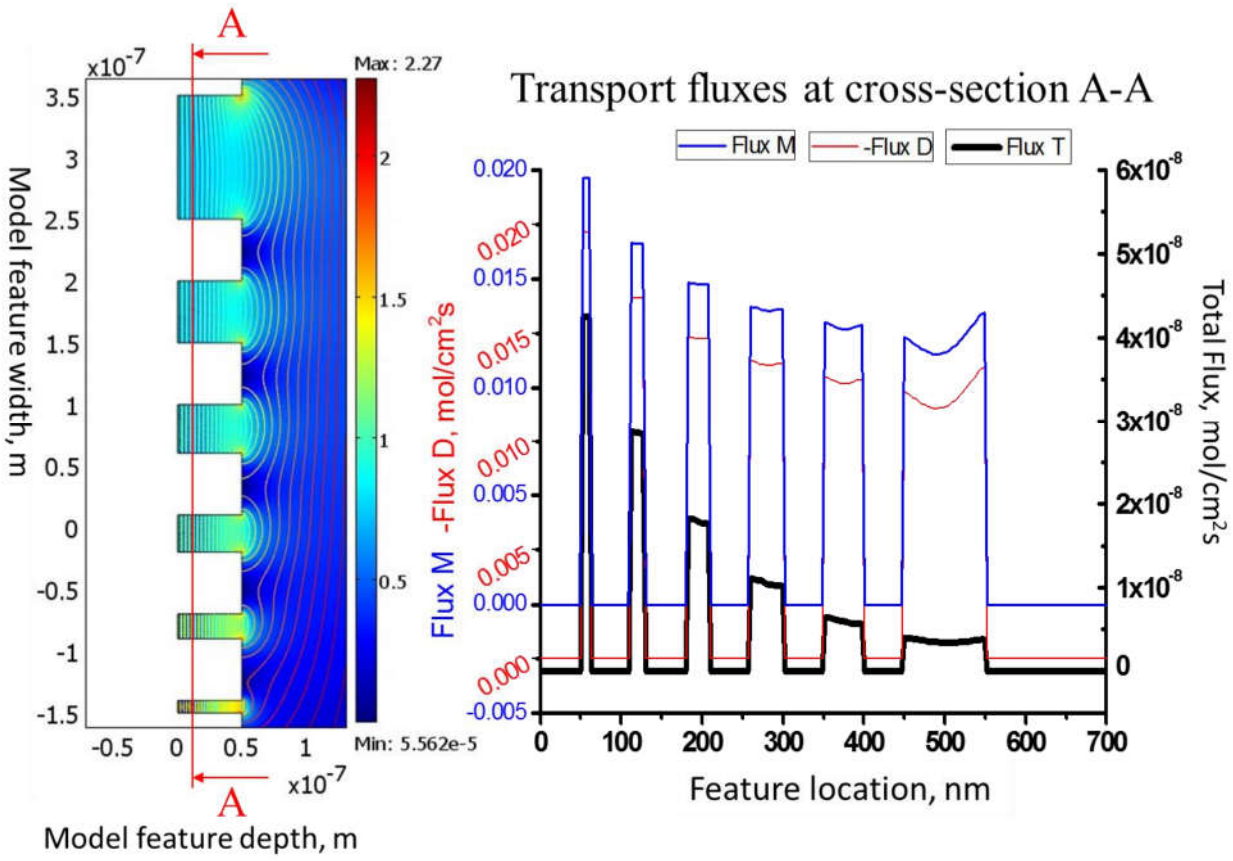

Fig. 8 Solid electrolyte domain size enhancement effect on ionic transport.

6. TABLES

Table 1 list of modeling parameters

Constant	*Value*	*Remarks*	*Remarks*
T	25+273.15	absolute temperature, K	
R	8.3145	universal gas constant (J/(mole*K))	
D_ag	1.4e-2*exp((-11100*4.18)/(R*T))	diffusivity of silver in silver sulfide, m^2/s	Ref. 1
u_ag	D_ag/(R*T)	mobility of silver in silver sulfide, s.mol/kg	
R_et	R_et for 0<t<100, R_et from figure 2.XXX	silver ion influx boundary condition, $mol/m^2.s$	Note
c0	33.532	intrinsic ion concentration, $mole/m^3$	Note
Nav	6.02E+23	Avogadro's number	
k	8.62E-05	Boltzmann's Constant, eV/K	
epsilon	8.8	dielectric constant, Ag_2S	Ref. 3
Vp	0.4	applied voltage, volt	
F	96485.34	Faraday's Constant	
sigma_e	1.00E-01	intrinsic electronic conductivity, S/m	Ref. 4

7. REFERENCE

[1] K. Terabe, M. Aono, Quantized conductance atomic switch, Nature, Vol. 433, 6, pp 47-50, 2005

[2] V. Jovanovic and M. Jovanovic, The behavior of mixed metal sulfide/silver sulfide sensing materials in solutions of silver ions, Ana. Chimica Acta, 176, pp285-289, 1985

[3] J. Han, Application of miniaturized electrochemical probes to nonisothermal transport studies in Ag2S, Solid State Ionics 81, pp119-127, 1995

[4] Ali Eftekhari, Chemical sensor based on silver / silver sulfide microelectrodes, Analytical Letters, 34, pp1087-1095, 2001

[5] A. Kryukov, A. S. Ya. Kuchmii, Optical and catalytic properties of Ag2S nanoparticles, Journal of Moleculer Catalysis A: Chemical, 221, pp209-221, 2004

[6] K Terabe, M. Aono, Ionic/electronic mixed conductor tip of a scanning tunneling microscope as ametal atom source or nanostructuring, Applied Physics Letters, Vol. 80, Num. 21, pp4001-4009, 2002

[7] K. Hsu, P Ferreira, N. Fang, Electrochemical Nanoimprinting with Solid-State Superionic Stamps , Nano Lett., Vol. 7 No. 2, 446-451, 2007

[8] Schultz P., Hsu, K., Fang, N., and, Ferreira, P., Journal of Vacuum Science & Technology B: Microelectronics and Nanometer Structures, Vol. 25, Issue 6, pp. 2419-2424, 2007

[9] Keng H. Hsu, Peter L. Schultz, Placid M. Ferreira, and Nicholas X. Fang, Exploiting transport of guest metal ions in a host ionic crystal lattice for nanofabrication: Cu nanopatterning with Ag2S, Applied Physics A, 10.1007/s00339-009-5344-6

[10] Hsu K. H., P. L. Schultz, N. X. Fang and P. M. Ferreira," Electrochemical Nanoimprinting of Silver and Copper with the Solid-State Superionic Stamping (S4) process," Unconventional Patterning Techniques and Applications, John Rogers and Hong H. Lee, eds, John Wiley and Sons, 2008.

[11] S. Miyatani, On the polarization of silver sulfide, Journal of the Physical Society of Japan, Vol. 10, No. 9, pp. 786-793, 1955

[12] H. Kwon, U. Ravaioli, Simulation of electronic/ionic mixed condection in solid ionic memory devices, Microelectronics Journal, 37, pp.1047-1051, 2006

[13] J. Janek, Oscillatory kinetics at solid/solid electrolyte boundaries in ionic crystals, Solid State Ionics, 131, pp.129-142, 2000

[14] J. D. Porter, Timothy O. Robinson, Surface diffusion of silver at the silver (111)/liquid-water interface from electrocrystallization measurements, J. Phys. Chem., 97 (25), pp 6696–6709, 1993

[15] P. N. I., Ecangelakis G. A., Kallinteris S. G., Molecular dynamics description of silver adatom diffusion on Ag(100) and Ag(111) surfaces, Computational materials science, vol. 10, no 1-4 pp. 105-110, 1998

[16] Byung D. Y. and Matthias S., Ab initio study of step formation and self-diffusion on Ag (100), Physical Review B, Vol. 55, 13916-13924, 1997

[17] J. Corish, M. T. Duffy and the late C. D. O'Briain, Electrochemical study of incorporation of silver vapour into -silver sulphide, Transactions of Faraday Society, 1971, 67, 1447 – 1452

Figure1

Click here to download high resolution image

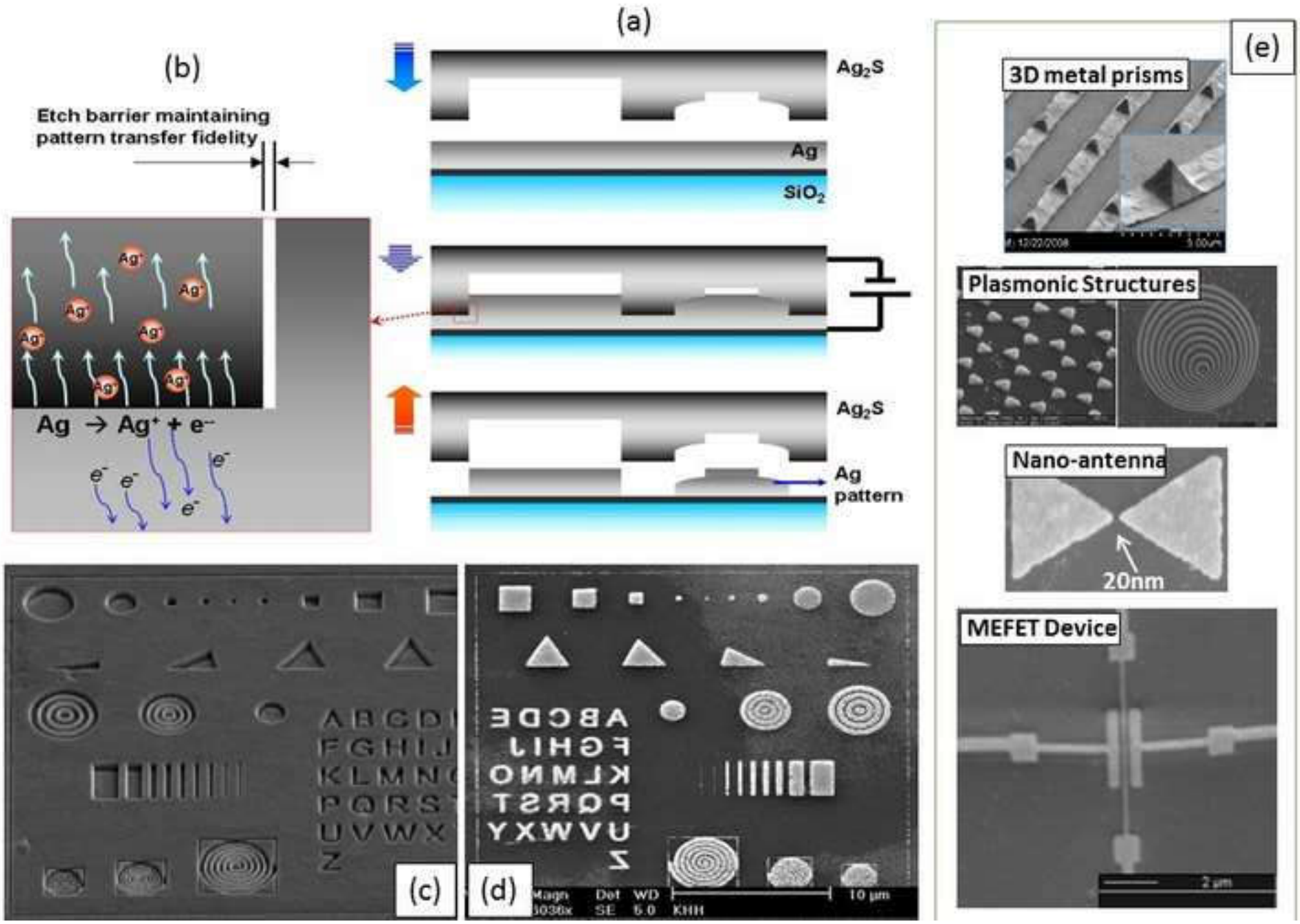

Figure2
Click here to download high resolution image

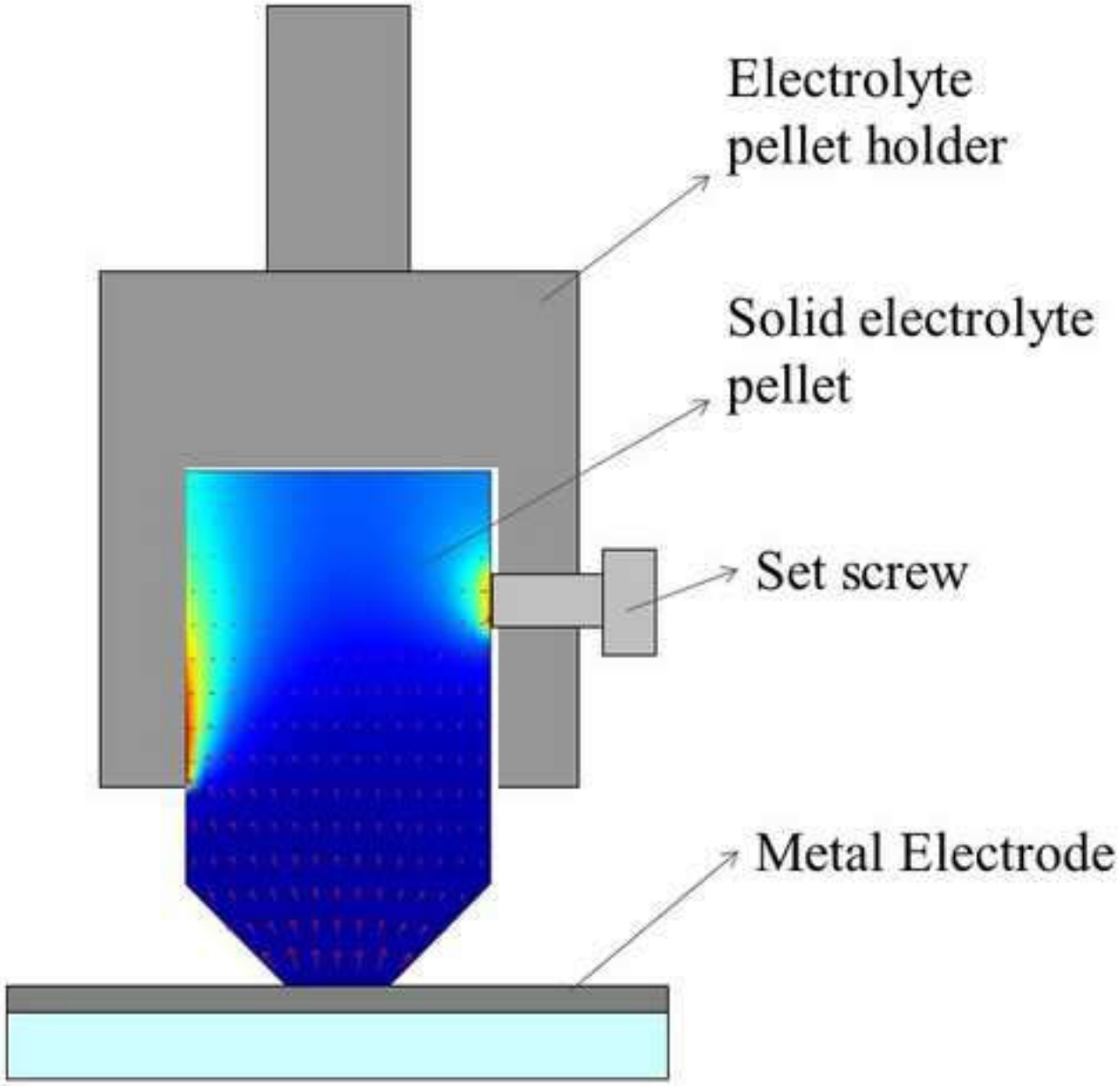

Figure3
Click here to download high resolution image

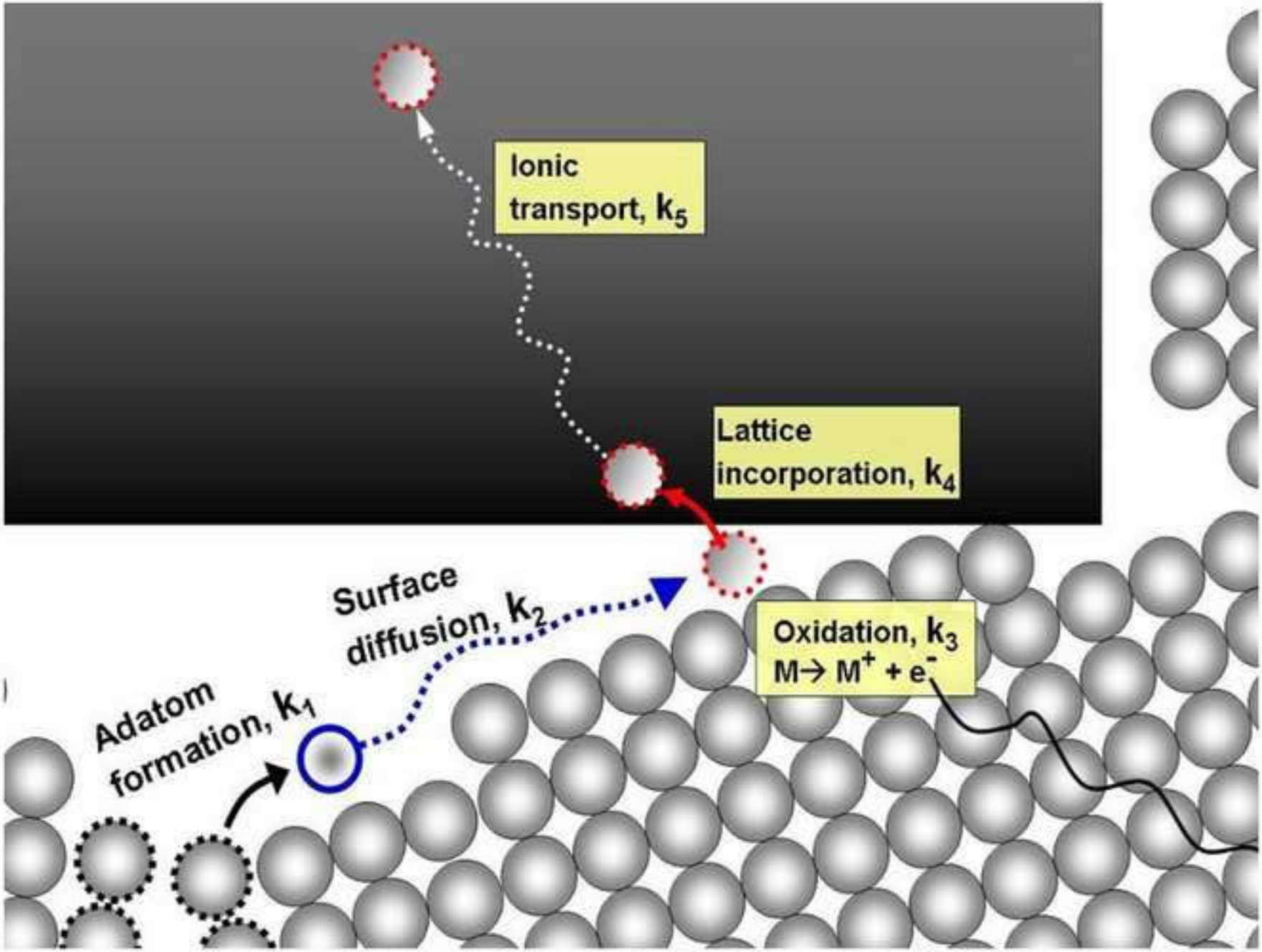

Figure4
Click here to download high resolution image

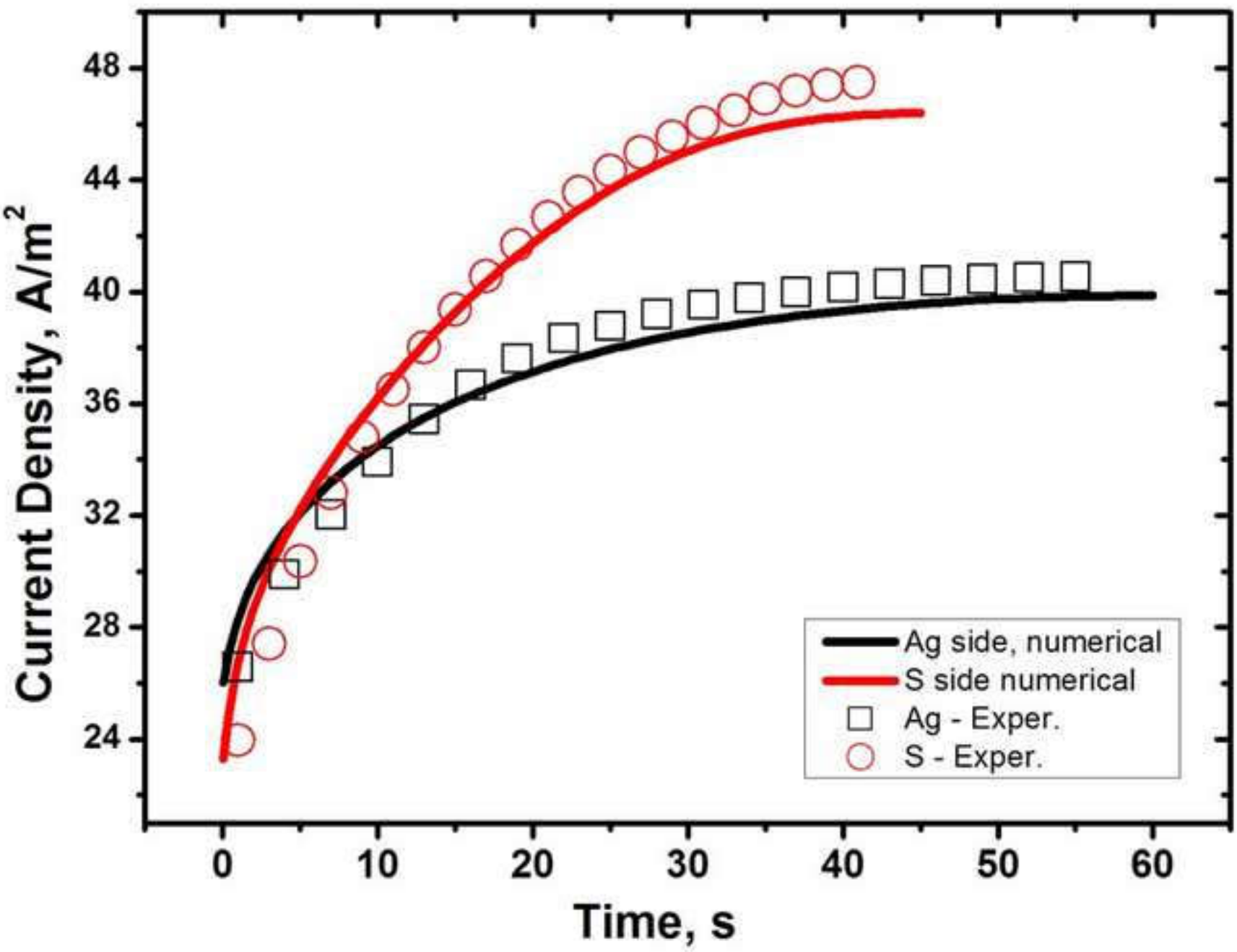

Figure 5

Click here to download high resolution image

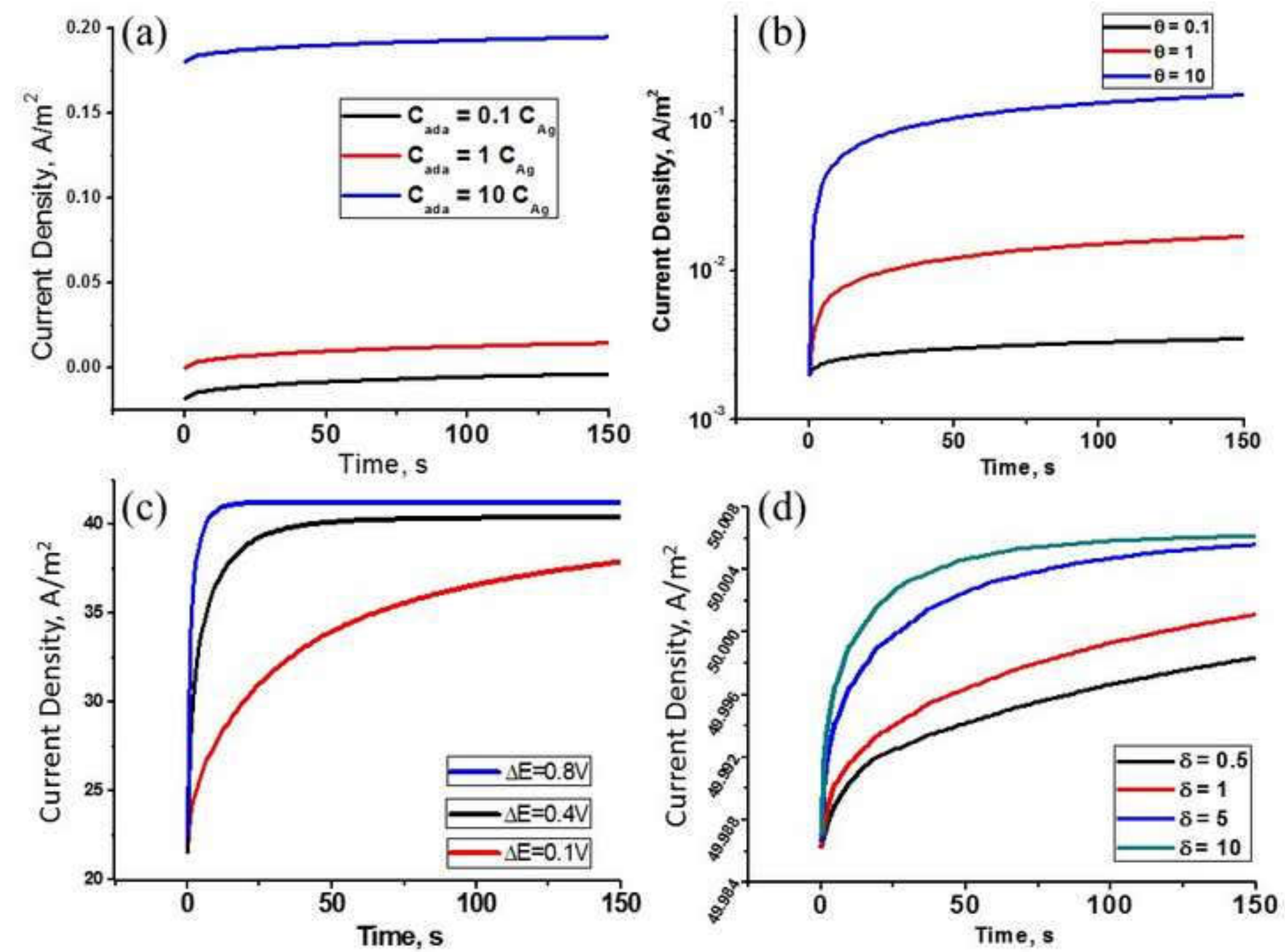

Figure6

Click here to download high resolution image

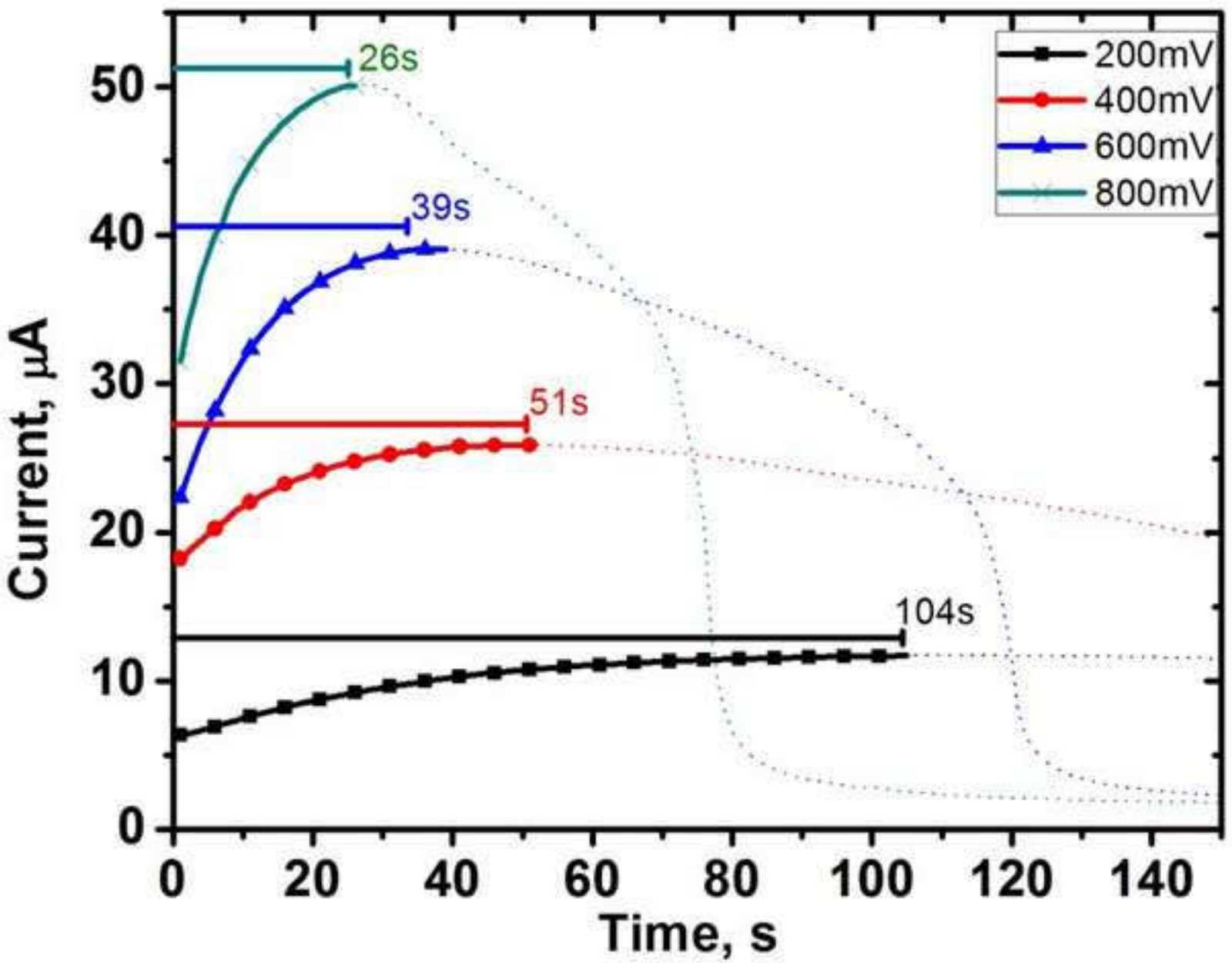

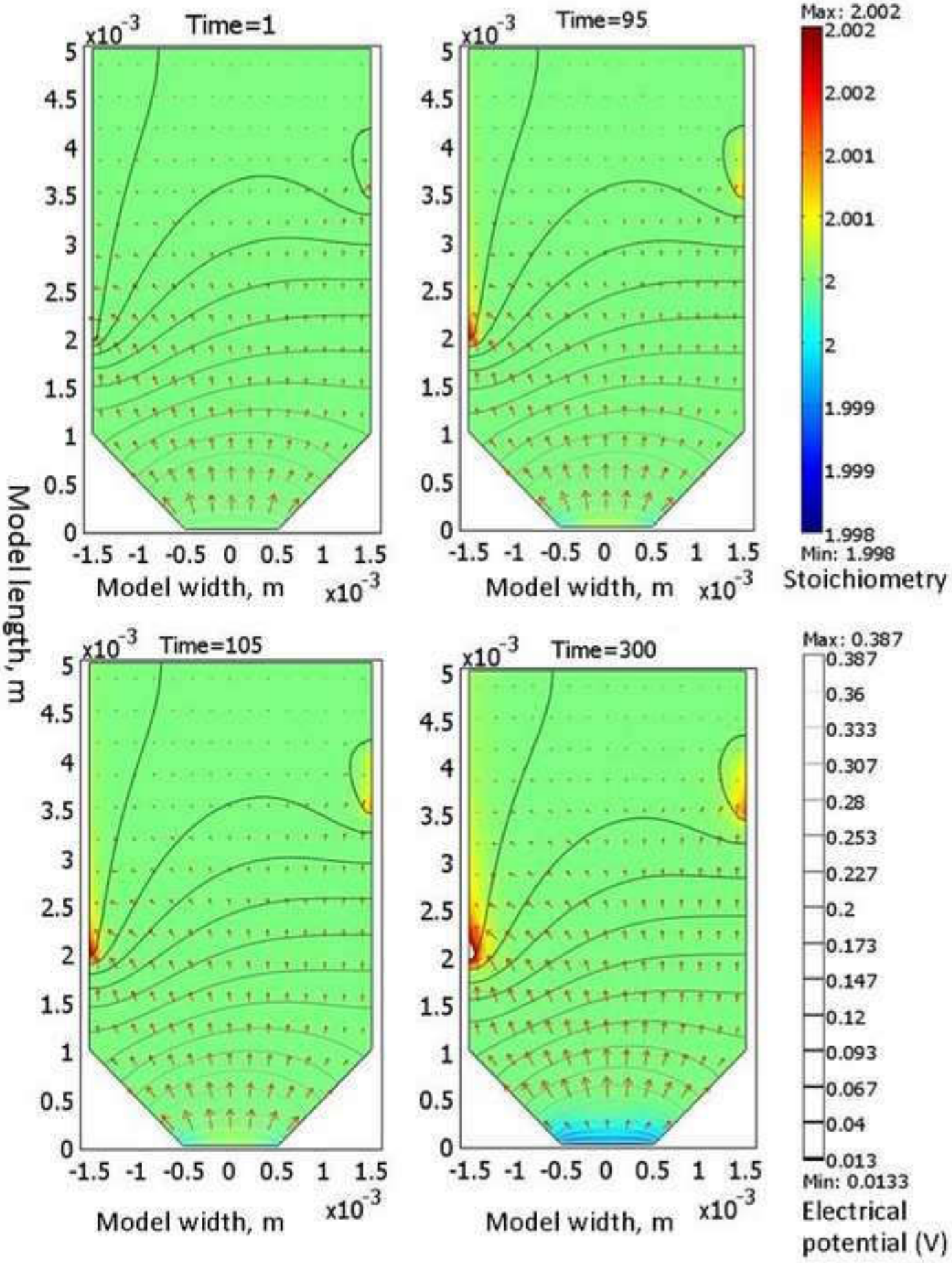

Figure 7
Click here to download high resolution image

Figure 8

Click here to download high resolution image

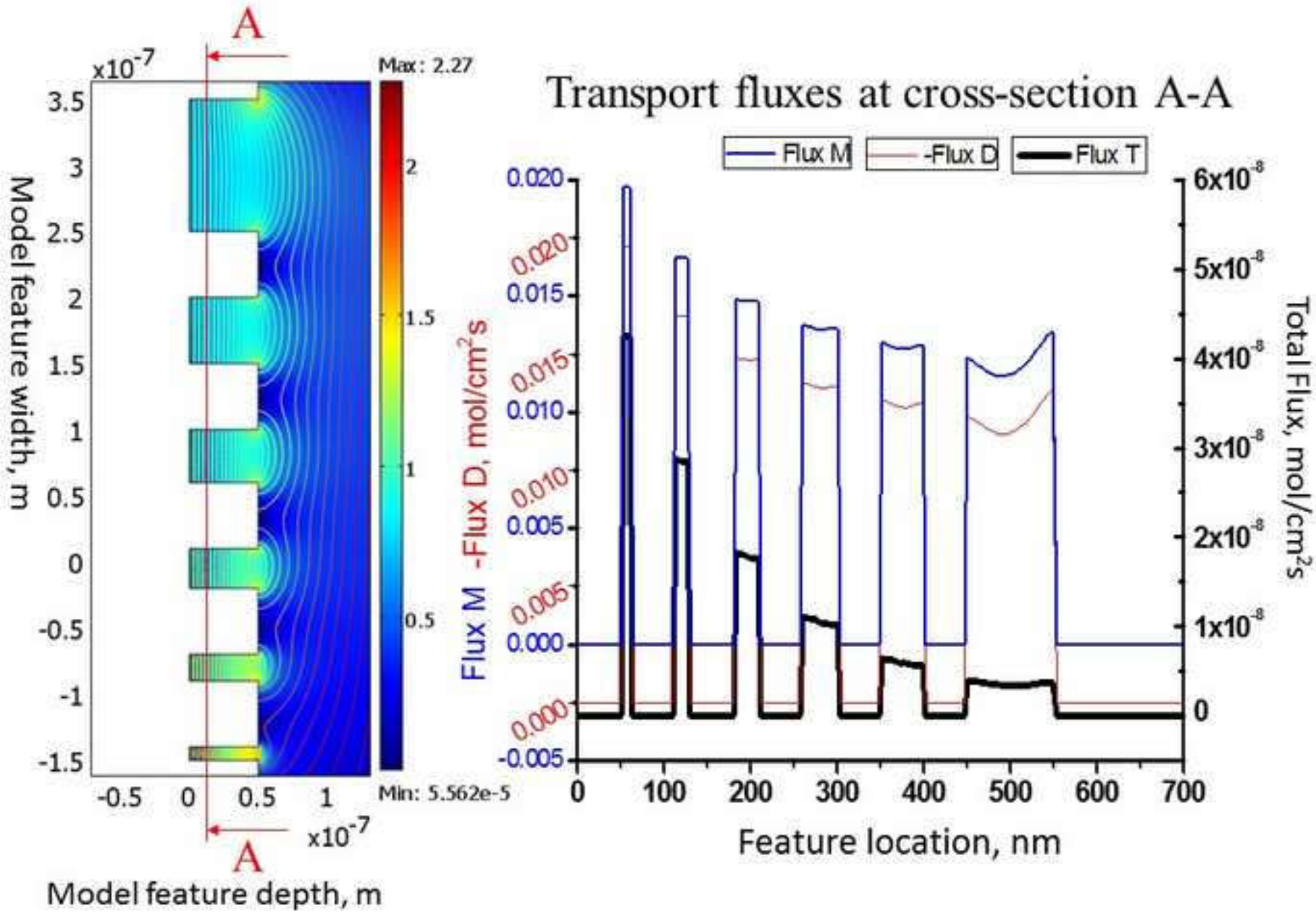

TABLES

Table 1 list of modeling parameters

Constant	*Value*	*Remarks*	*Remarks*
T	25+273.15	absolute temperature, K	
R	8.3145	universal gas constant (J/(mole*K))	
D_ag	1.4e-2*exp((-11100*4.18)/(R*T))	diffusivity of silver in silver sulfide, m^2/s	Ref. 1
u_ag	D_ag/(R*T)	mobility of silver in silver sulfide, s.mol/kg	
R_et	R_et for 0<t<100, R_et from figure 2.XXX	silver ion influx boundary condition, $mol/m^2.s$	Note
c0	33.532	intrinsic ion concentration, $mole/m^3$	Note
Nav	6.02E+23	Avogadro's number	
k	8.62E-05	Boltzmann's Constant, eV/K	
epsilon	8.8	dielectric constant, Ag_2S	Ref. 3
Vp	0.4	applied voltage, volt	
F	96485.34	Faraday's Constant	
sigma_e	1.00E-01	intrinsic electronic conductivity, S/m	Ref. 4